THE ASTROPHYSICAL JOURNAL, 426:L51–L54, 1994 May 1

EXTREME ULTRAVIOLET EXPLORER SATELLITE OBSERVATION OF JUPITER'S IO PLASMA TORUS

D. T. HALL,[1] G. R. GLADSTONE,[2] H. W. MOOS,[1] F. BAGENAL,[3] J. T. CLARKE,[4] P. D. FELDMAN,[1]
M. A. MCGRATH,[5] N. M. SCHNEIDER,[3] D. E. SHEMANSKY,[6] D. F. STROBEL,[1] AND J. H. WAITE[2]

Received 1993 November 16; accepted 1994 February 16

ABSTRACT

We present the first *Extreme Ultraviolet Explorer* satellite observation of the Jupiter system, obtained during the 2 day period 1993 March 30 through April 1, which shows a rich emission-line spectrum from the Io plasma torus spanning wavelengths 370 to 735 Å. The emission features correspond primarily to known multiplets of oxygen and sulfur ions, but a blended feature near 372 Å is a plausible Na II transition. The summed detected energy flux of $(7.2 \pm 0.2) \times 10^{-11}$ ergs cm^{-2} s^{-1} corresponds to a radiated power of $\approx 4 \times 10^{11}$ W in this spectral range. All ansa emissions show a distinct dawn-dusk brightness asymmetry and the measured dusk/dawn ratio of the bright S III λ680 feature is 2.3 ± 0.3, significantly larger than the ratio measured by the *Voyager* spacecraft UV instruments. A preliminary estimate of ion partitioning indicates that the oxygen/sulfur ion ratio is ≈ 2, compared to the value ≈ 1.3 measured by *Voyager*, and that $[Na^+]/[e] > 0.01$.

Subject headings: line: identification — planets and satellites: individual (Io, Jupiter) — plasmas — ultraviolet: solar system

1. INTRODUCTION

In 1979, the *Voyager* Ultraviolet Spectrographs (UVS) detected extreme ultraviolet (EUV) radiation from a toroidal volume centered on Io's orbit generated by electron-impact excitation of oxygen and sulfur ions with the brightest feature near 680 Å, a blend of S III emission lines (Broadfoot et al. 1979; Shemansky & Smith 1981). In addition, the *Voyager* Plasma Science (PLS) instruments obtained in situ measurements of ions and electrons (Bridge et al. 1979; Bagenal & Sullivan 1981; Bagenal et al. 1985; Sittler & Strobel 1987), making the Io torus one of the best characterized astrophysical plasmas. The Io torus therefore provides an important benchmark for EUV plasma diagnostic techniques in general. However, during the 14 year period after the *Voyager* encounters, the only EUV Io torus observations acquired were two short-duration spectra obtained by the Hopkins Ultraviolet Telescope during the *Astro-1* shuttle mission in 1990 December (Moos et al. 1991; Hall et al. 1994). In this *Letter* we present the first observation of the Io plasma torus performed by the *Extreme Ultraviolet Explorer* (*EUVE*) satellite.

2. THE *EUVE* INSTRUMENTATION AND IO TORUS OBSERVATION

EUVE is a NASA explorer-class satellite launched in 1992 June into a 520 km circular orbit. Its payload includes three EUV spectrographs covering 70–750 Å with resolving power 200–400. Each spectrograph has a roughly circular field of view 300′ in diameter and employs a stack of three microchannel plate detectors backed by conducting anodes that provide imaging information as well as the capability to determine individual photon-event detection times (Finley et al. 1988; Hettrick et al. 1985; Siegmund et al. 1984). Photons are spectrally dispersed along the x-pixel direction, and the instrument provides spatial imaging in the y-direction. Each y-pixel spans 4.″36, and the point-source spatial resolution is $\approx 42''$ FWHM. Raw data from each spectrograph consists of a series of time-tagged photoevents $\{t, x, y\}$, each indicating a count registered at time t at detector coordinates (x, y). Event times are accurate to ≈ 8 ms. Detector pixel coordinates are corrected for geometrical distortions, spectral dispersion nonlinearities and other instrumental effects (Vallerga et al. 1989). Moving targets require a further correction to account for the changing aspect of the spacecraft. Images and spectra are generated by binning the time-tagged counts in x and y, and various time filters may be applied during the binning process to investigate flux variations.

The Jupiter observation was performed during several consecutive spacecraft orbits between 1993 March 30, 15:15 UT and April 1, 15:16 UT. The long-wavelength spectrograph was exposed for a total duration of 62,196 s and detected several Io plasma torus emission lines between 370 and 735 Å. No torus emissions were detected at shorter wavelengths in the other two detectors. Figure 1 shows the detected spectrum and a best-fit model spectrum, along with emission line identifications (see § 3 for spectral analysis details). Figure 2 (Plate L5) shows the spatial profiles of two of the brighter spectral features, S III λ680 and O II λ539, each showing that emissions from dusk ansa of the Io torus are distinctly brighter than those from the dawn ansae (see § 4). The average Earth-Jupiter distance was 4.45 AU, and one equatorial Jupiter radius ($1R_J = 71{,}400$ km) spanned 22.″1. Interplanetary absorption of EUV emissions is negligible because of extremely low hydrogen column densities between Jupiter and Earth ($N_H < 10^{13}$ cm^{-2}).

During the observation, the spacecraft orientation was adjusted once each orbit according to a calculated ephemeris to point the telescope boresight directly at Jupiter, and maintain a role angle such that photons were dispersed in the long-

[1] Center for Astrophysical Sciences, Department of Physics and Astronomy, The Johns Hopkins University, Baltimore, MD 21218.
[2] Department of Space Sciences, Southwest Research Institute, San Antonio, TX 78228.
[3] Department of Astrophysical, Planetary and Atmospheric Sciences, University of Colorado, Boulder, CO 80309.
[4] Department of Atmospheric and Oceanic and Space Sciences, University of Michigan, Ann Arbor, MI 48109.
[5] Space Telescope Science Institute, 3700 San Martin Drive, Baltimore, MD 21218.
[6] Aerospace Engineering Department, University of Southern California, Los Angeles, CA 90089.

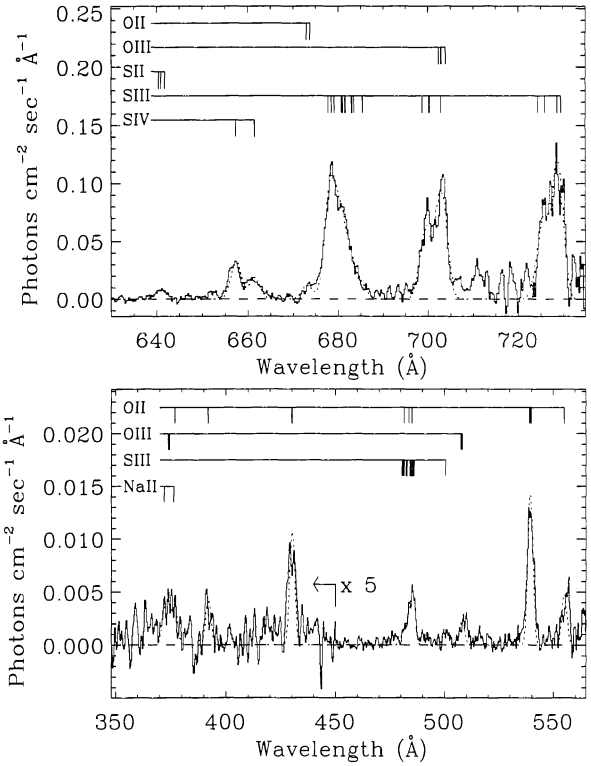

FIG. 1.—*EUVE* long-wavelength detector spectrum of the Io plasma torus. The solid line shows the detected flux from the entire torus, except the fraction obscured by Jupiter, smoothed over 3 pixels. For $\lambda < 450$ Å, the data are multiplied by 5 and smoothed over 5 pixels. Emitting ions and laboratory-measured line wavelengths are shown above the spectra. The dotted line shows a preliminary best-fit model spectrum.

wavelength spectrograph along the direction of the planetary spin axis. With this scheme, the imaging capabilities of the instrument were optimized to detect structure along Io's projected orbital ellipse. The detected torus emissions span ≈ 100 y-pixels, or ≈ 7.3. The nominal boresight of the long-wavelength detector is at $y = 1024$, but may not be constant as a function of wavelength and is known to vary with thermally induced spacecraft flexure. Additional uncertainties in boresight y may be caused by spacecraft jitter and ephemeris errors. Because of these uncertainties, the absolute position of the spatial scale in Figure 2 (determined assuming a boresight $y = 1033$) is accurate to $\pm 1.7 R_J$, but may improve with further analysis.

To investigate flux variations during the 2 day observation period, the time-tagged counts are binned into eight sequential 6 hr periods, each representing ≈ 8000 s of accumulated exposure time. Statistically significant trends are apparent for only two of the features. The S III λ680 flux increased by $\approx 20\%$ during the observational period. The S II λ640 flux varied in a roughly sinusoidal fashion, with a minimum-to-maximum ratio of $\approx 4 \pm 2$, and a period roughly coincident with Io's orbital period. However, because the observation spanned 1.1 Io orbital periods, possible Io-correlated flux variations are difficult to distinguish from unrelated variations having a similar timescale. Additional data are required to investigate Io correlated flux modulations of the type observed by the *Voyager* UVS instruments (Sandel & Broadfoot 1982b). Flux variations correlated with Jupiter's ≈ 10 hr rotational period are investigated by accumulating the time-tagged photon counts into eight Jovian System III central meridian longitude (CML) bins. For all of the features, observed CML flux variations are competitive with statistical uncertainties; CML variations in S III λ680 and O II λ539 fluxes have amplitude $\leq 20\%$.

3. SPECTRAL ANALYSIS

Figure 1 shows the full 62,196 s spectrum with background and instrument dark counts removed and represents the emissions from the entire torus, except the fraction obscured by Jupiter. Preliminary identification of emitting ions with laboratory-measured wavelengths are shown above the spectrum. The dotted line shows a preliminary best-fit model spectrum. Between 565 and 630 Å no torus emissions were detected, possibly because the signal-to-noise ratio is degraded by elevated count rates associated with the bright terrestrial He I λ584 feature. Total fluxes of individual features are given in Table 1. The energy flux obtained by integrating over the observed spectrum is $(7.2 \pm 0.2) \times 10^{-11}$ ergs cm^{-2} s^{-1}, where the 1 σ variance is due to statistical measurement uncertainty. This corresponds to a radiated power of 4×10^{11} W. The three strongest features in the 671–731 Å range account for $\approx \frac{2}{3}$ of the detected power.

Some emission features in Figure 1 clearly show blended, multiline structure. We investigate spectral content and wavelength calibration using a spectral fitting procedure, where synthetic spectra of individual lines and multiplets are correlated with the observed spectrum. Because *Voyager* spacecraft observations indicate that Io torus composition is dominated by oxygen and sulfur ions (Shemansky & Smith 1981), we restrict our analysis to the known strong transitions of these ions and use laboratory-measured vacuum wavelengths. The weak and blended feature in the 370–380 Å range requires an emission line at ≈ 372 Å, which may be identified as Na II emission. The analysis indicates an effective spectral resolution of 2.5–3.5 Å (Gaussian FWHM), due to the intrinsic instrument spectral resolution and the average spatial extent of the torus along Jupiter's spin axis. From the best-fit model spectrum we estimate the percentage contribution of individual transitions to the observed emission features (see Table 1). Approximately 82% of the detected power is accounted for in the best-fit spectrum. The unaccounted portion is mostly due to unfit features in the 705–735 Å region, where the signal-to-noise is degraded by lower instrument sensitivity.

For the 350–565 Å range, the analysis indicates that the current nominal wavelength calibration is correct to within measurement uncertainty, and there is a linear relationship between image x-pixels and wavelength. Near the edge of the long-wavelength detector ($\lambda > 628$ Å), where the current wavelength scale is known to suffer from residual nonlinearities (Olsen 1993), we have calculated a preliminary revised scale (used in Fig. 1) with a quadratic adjustment.

4. DAWN-DUSK BRIGHTNESS ASYMMETRY

Figure 2 shows the distribution of flux for two spectral features. In the top panel, a false color image of the S III λ680 feature is shown with a cartoon of Jupiter and Io's orbit drawn to scale below. O II λ539 emission is shown in the lower image. Wavelengths spanned by each feature are shown to the left of each image. The bottom panel shows the flux summed along the direction perpendicular to the planetary equator for the two features. A striking dawn-dusk ansa brightness asymmetry is clearly evident for both features, and similar asymmetries are apparent in all of the other features. Defining the ansa emissions as the integrated signal between 5 and $6 R_J$, the dusk/dawn ansa flux ratios are 2.3 ± 0.3 and 2.7 ± 0.5 respectively for the S III and O II features plotted in Figure 2.

TABLE 1

EUVE Io Plasma Torus Emission Features

λ(Å)	Flux[a]	Ion[b]	Transition(s)[b]	%[c]	Ref.[d]
370–380	$(5.94 \pm 0.94)^{-3}$	NaII	$2p^6\ g^1S_0 - 3s\ 1/2[1/2]_1$	30	1
		NaII	$2p^6\ g^1S_0 - 3s\ 3/2[3/2]_1$	?[e]	1
		OII	$2p^3\ g^4S^o - 5d\ ^4P^o$	?[e]	1
		OIII	$2p^2\ g^3P - 3s\ ^3P^o$	?[e]	1
389–395	$(2.46 \pm 0.72)^{-3}$	OII	$2p^3\ g^4S^o - 4d\ ^4P$	100	1
426–434	$(8.04 \pm 0.91)^{-3}$	OII	$2p^3\ g^4S^o - 3d\ ^4P$	100	1
480–489	$(2.18 \pm 0.13)^{-2}$	SIII	$3p^2\ g^3P - 4d\ ^3P$	?[e]	2
		SIII	$2p^2\ g^3P - 4d\ ^3D$	?[e]	2
		OII	$2p^3\ ^2D^o - 3d\ ^2D$	?[e]	1
		OII	$2p^3\ ^2D^o - 3d\ ^2P^o$	?[e]	1
		OII	$2p^3\ ^2D^o - 3d\ ^2F$	?[e]	1
505–512	$(1.03 \pm 0.13)^{-2}$	OIII	$2p^2\ g^3P - 2p^3\ ^3S^o$	100	1
536–543	$(4.78 \pm 0.22)^{-2}$	OII	$2p^3\ g^4S^o - 3s\ ^4P$	100	1
552–559[f]	$(1.84 \pm 0.26)^{-2}$	OII	$2p^3\ ^2D^o - 3s\ ^2D$	?	1
		OIII	$2p^3\ ^3D^o - 3p\ ^3P$	?	1
		SIV	$3p\ g^2P^o - 4s\ ^2S$	?	1
639–643	$(2.33 \pm 0.36)^{-2}$	SII	$3p^3\ g^4S^o - 4d\ ^4P$	100	3
654–665	$(1.62 \pm 0.09)^{-1}$	SIV	$3p\ g^2P^o - 3d\ ^2D$	100	1
671–685	$(6.26 \pm 0.18)^{-1}$	SIII	$3p^2\ g^3P - 3d\ ^3D^o$	75	2
		SIII	$3p^2\ g^3P - 4s\ ^3P^o$	20	2
		OII	$2p^3\ ^2P^o - 3s\ ^2P$	5	1
697–705	$(4.84 \pm 0.22)^{-1}$	SIII	$3p^2\ g^3P - 3d\ ^3P^o$	?[e]	2
		OIII	$2p^2\ g^3P - 2p^3\ ^3P^o$	?[e]	1
724–731	$(5.75 \pm 0.49)^{-1}$	SIII	$3p^2\ g^3P - 3p^3\ ^3S$	90	2
		SIII	$3p^2\ ^1D - 4s\ ^1P$	10	2

[a] Total detected flux and 1 σ uncertainty in photons $cm^{-2}\ s^{-1}$. Superscripts denote powers of ten: $(5.94 \pm 0.94)^{-3} = (5.94 \pm 0.94) \times 10^{-3}$.

[b] Ions and transitions contributing to identified feature. Transitions are denoted with lower energy states first. Ground states are preceded with the letter g.

[c] Preliminary estimate of the percentage contribution of the transition to the total detected flux.

[d] Reference for laboratory transition identification.

[e] These transitions are severely blended.

[f] This feature is possibly adversely affected by high background rates associated with the relatively wide and bright terrestrial He I λ584 feature.

References.—(1) Kelly 1987. (2) Johansson et al. 1992. (3). Pettersson 1983.

5. ION PARTITIONING

Electron impact dominates torus EUV line excitation and line brightnesses depend sensitively on the mean energy of the torus electrons (Shemansky & Smith 1981). An accurate determination of emitting ion abundances therefore necessarily relies on a good description of the effective temperature of electrons. The *EUVE* torus spectrum contains several multiplets suitable for determining the effective electron temperature, but many are severely blended or require electron impact excitation rates not currently available. We therefore defer a detailed analysis to determine effective electron temperature.

To obtain a rough estimate of ion partitioning we characterize the energy distribution of torus electrons using *Voyager 1* spacecraft in situ measurements and explore the implied limits of the ion mixing ratios. Torus EUV emissions originate from the region between 5.4 and 7.0R_J, where *Voyager 1* observed a two-component electron gas: a cold component with T_e = 4–8 eV and a hot component (≈200 eV) with a mixing ratio of less than 0.5% (Sittler & Strobel 1987; Bagenal 1994). Using these observations as a guideline, we assume that reasonable bounds on the temperature of cold electrons is 3–10 eV and that the hot electron mixing ratio is less than 1%. These bounds imply a range of possible mixing ratios for each ion (given in Table 2, col. [2]), indicating the sensitivity of the partitioning analysis to the electron parameters. The derived lower limit for the Na^+ mixing ratio is 0.01. Also in Table 2 (col. [3]), we tabulate partitioning assuming an electron temperature of 5 eV and excluding Na^+, to facilitate comparison to previous analyses using similar assumptions. Mixing ratios in Table 2 are derived assuming a homogeneous charge neutral plasma, and are based on the strongest and least-blended multiplets for each ion. Emission rates are calculated using the collision strengths given in Table 2, assuming electron-impact excitation from the ground term and neglecting cascade contributions. Because only relative multiplet fluxes are modeled, the calculation to derive the ion mixing ratios is independent of absolute electron density.

6. DISCUSSION AND CONCLUSIONS

During the *EUVE* observation the Io torus was radiating $\approx 4 \times 10^{11}$ W in several emission multiplets in the 370–735 Å region. A preliminary analysis based on the Shemansky (1987) torus emission model suggests that comparable power is radiated in the 735–1260 Å range, and longer wavelength emissions contribute significantly as well. However, a detailed model analysis similar to that of Shemansky & Smith (1981) is required to estimate the power radiated at all wavelengths from the entire torus during the *EUVE* observation. The results will depend critically on the effective electron temperature in the torus, which has yet to be determined from these data. In addition, because the derived ion partitioning depends on electron temperature, the estimates given in Table 2 must be regarded as preliminary. Estimates of the power

TABLE 2

EUVE Io Plasma Torus Ion Partitioning

Ion	Mixing Ratio[a]		λ (Å)[b]	Flux[c]	Ω[d]	*Voyager*[e]	Other
	Range	$T_e = 5$ eV					
O^+	0.44–0.66	0.55	539	4.8^{-2}	0.4	0.40	0.27[f], 0.37[g], 0.26[h]
O^{2+}	0.008–0.017	0.012	508	1.0^{-2}	5.2	<0.02	0.016[f], 0.034[i]
S^+	0.08–0.15	0.13	640	2.3^{-2}	0.4	0.17	0.18[f], 0.14[g]
S^{2+}	0.06–0.17	0.11	678	6.0^{-1}	22	0.18	0.22[f], 0.20[g]
S^{3+}	0.016–0.036	0.026	658	1.6^{-1}	19	≤0.02	0.04[f], 0.03[g]
Na^+	>0.01		372	1.8^{-3}	0.23	<0.03	

[a] Mixing ratios are ion number densities relative to the total electron density. The quoted ranges are derived by assuming excitation by a two-component electron gas: a cold component with 3 eV ≤ T_e ≤ 10 eV and hot component (200 eV) with mixing 0%–1%. Mixing ratios for a sulfur and oxygen plasma excited by isothermal electrons (5 eV) are also tabulated.

[b] Central wavelength of transition(s) used to estimate ion mixing ratio.

[c] Flux of transition(s) in photons $cm^{-2}\ s^{-1}$. Superscripts denote powers of 10: $4.8^{-2} = 4.8 \times 10^{-2}$.

[d] Thermally averaged electron impact collision strength for combined transition(s). These are taken mostly from the electron-impact emission model (program COREQ) of Shemansky 1987; 1988 developed to analyze *Voyager* UVS torus spectra.

[e] *Voyager* mixing ratios taken from the unified PLS and UVS analysis (Bagenal 1994); quoted values are representative of the 5.7–6.0R_J region.

[f] Mixing ratios from *Hopkins Ultraviolet Telescope* observations (Moos et al. 1991).

[g] Mixing ratios from *International Ultraviolet Explorer* observations (McGrath et al. 1990).

[h] Mixing ratios from *Hubble Space Telescope* O II λ2471 observations (McGrath et al. 1993).

[i] Mixing ratio from ground-based O III λ5007 observations (Thomas 1993).

radiated at all wavelengths from the entire torus during the *Voyager* encounters are in the range 2–6 × 10^{12} W (Sandel et al. 1979; Shemansky & Smith 1981; Smith et al. 1988).

During both *Voyager* encounters, the UVS instruments conducted extensive scans of Io torus EUV emissions. Preencounter scans with spatial resolution comparable to that of *EUVE* consistently indicated well-defined peaks in flux at both dawn and dusk ansae (Sandel & Broadfoot 1982a). *Voyager* dusk/dawn brightness ratios for S III λ680 were variable, but generally within the range 1.1–1.6, and the asymmetry was attributed to a difference between the effective electron temperature of the two ansae (Shemansky & Sandel 1982), although electron density differences probably contribute as well (see Morgan 1985; Smyth & Combi 1987). The *EUVE* observation provides a striking confirmation of the continued existence of a dawn-dusk brightness asymmetry. However, the distribution of flux (bottom panel; Fig. 2) is significantly different than that observed by *Voyager*. While all of the features in the *EUVE* spectrum peak strongly at the dusk ansa, none show well-defined peaks at the dawn ansa. The *EUVE* S III λ680 dusk/dawn flux ratio of 2.3 ± 0.3 is notably larger than the *Voyager* value. While part of this difference may be due to different observing geometry, it suggests a significant change in the mechanisms creating the dawn-dusk asymmetry.

The preliminary *EUVE* ion partitioning analysis indicates that the dominant ion, O^+, is about half as abundant as torus electrons. S^+ and S^{2+} are also major components while S^{3+} and O^{2+} are relatively minor. The preliminary identification of Na II λ372 emission represents the first detection of sodium ions in the torus, and suggests that Na^+ is >0.01 as abundant as electrons. Relative to previous estimates of ion mixing ratios based on *Voyager* and other observations (see Table 2), the *EUVE* ion mixture is richer in O^+, and correspondingly poorer in S^+ and S^{2+}. Assuming an electron temperature of 5 eV, the *EUVE* analysis indicates that the ratio of oxygen to sulfur ions is ≈2, significantly larger than the *Voyager* ratio of ≈1.3 (Shemansky 1987). This may indicate a fundamental change in the mass source and loss processes that determine the torus oxygen/sulfur ratio. The larger O^+ mixing ratio would also moderately decrease the radiative cooling efficiency, since the ratio of oxygen/sulfur radiative cooling coefficients is ≈0.2 (Shemansky 1988).

The *EUVE* observation and analysis were supported by NASA grant NAG 52276 to The Johns Hopkins University. J. Clarke was supported by NASA grant NAGW-1766 to the University of Michigan.

REFERENCES

Bagenal, F. 1994, J. Geophys. Res., in press
Bagenal, F., & Sullivan, J. D. 1981, J. Geophys. Res., 86, 8447
Bagenal, F., et al. 1985, J. Geophys. Res., 90, 1755
Bridge, H. S., et al. 1979, Science, 204, 972
Broadfoot, A. L., et al. 1979, Science, 204, 979
Finley, D. S., Jelinsky, P., Bowyer, S., & Malina, R. F. 1988, Appl. Opt., 27, 1476
Hall, D. T., et al. 1994, ApJ, 420, L45
Hettrick, M. C., Bowyer, S., Malina, R. F., Martin, C., & Mrowka, S. 1985, App. Opt., 24, 1737
Johansson, L., Magnusson, C. E., Joelsson, I., & Zetterberg, P. O. 1992, Phys. Scripta, 46, 221
Kelly, R. L. 1987, J. Phys. Chem. Ref. Data, 16, Suppl. 1, 1
McGrath, M. A., Feldman, P. D., Strobel, D. F., Moos, H. W., & Ballester, G. E. 1993, ApJ, 415, L55
McGrath, M. A., Moos, H. W., Strobel, D. F., & Ballester, G. E. 1990, presented at the Fred Scarf Memorial Symposium, Magnetospheres of the Outer Planets, Annapolis, MD, unpublished
Moos, H. W., et al. 1991, ApJ, 382, L105
Morgan, J. S. 1985, Icarus, 63, 243
Olsen, E. 1993, *EUVE* Electronic Newsletter, 3, 1993 August 27
Pettersson, J. E. 1983, Phys. Scripta, 28, 421
Sandel, B. R., & Broadfoot, A. L. 1982a, J. Geophys. Res., 87, 212
———. 1982b, J. Geophys. Res., 87, 2231
Shemansky, D. E. 1987, J. Geophys. Res., 92, 6141
———, 1988, J. Geophys. Res., 93, 1773
Shemansky, D. E., & Sandel, B. R. 1982, J. Geophys. Res., 87, 219
Shemansky, D. E., & Smith, G. R. 1981, J. Geophys. Res., 86, 9179
Siegmund, O. H. W., Malina, R. F., Coburn, K., & Werthimer, D. 1984, IEEE Trans. Nucl. Sci., NS-31, 776
Sittler, E. C., & Strobel, D. F. 1987, J. Geophys. Res., 92, 5741
Smith, R. A., Bagenal, F., Cheng, A. F., & Strobel, D. F. 1988, Geophys. Res. Lett., 15, 545
Smyth, W. H., & Combi, M. R. 1987, Geophys. Res. Lett., 14, 973
Thomas, N. 1993, ApJ, 414, L41
Vallerga, J. V., Kaplan, G. C., Siegmund, O. H. W., Lampton, M., & Malina, R. F. 1989, IEEE Tran. Nucl. Sci., 36, 881

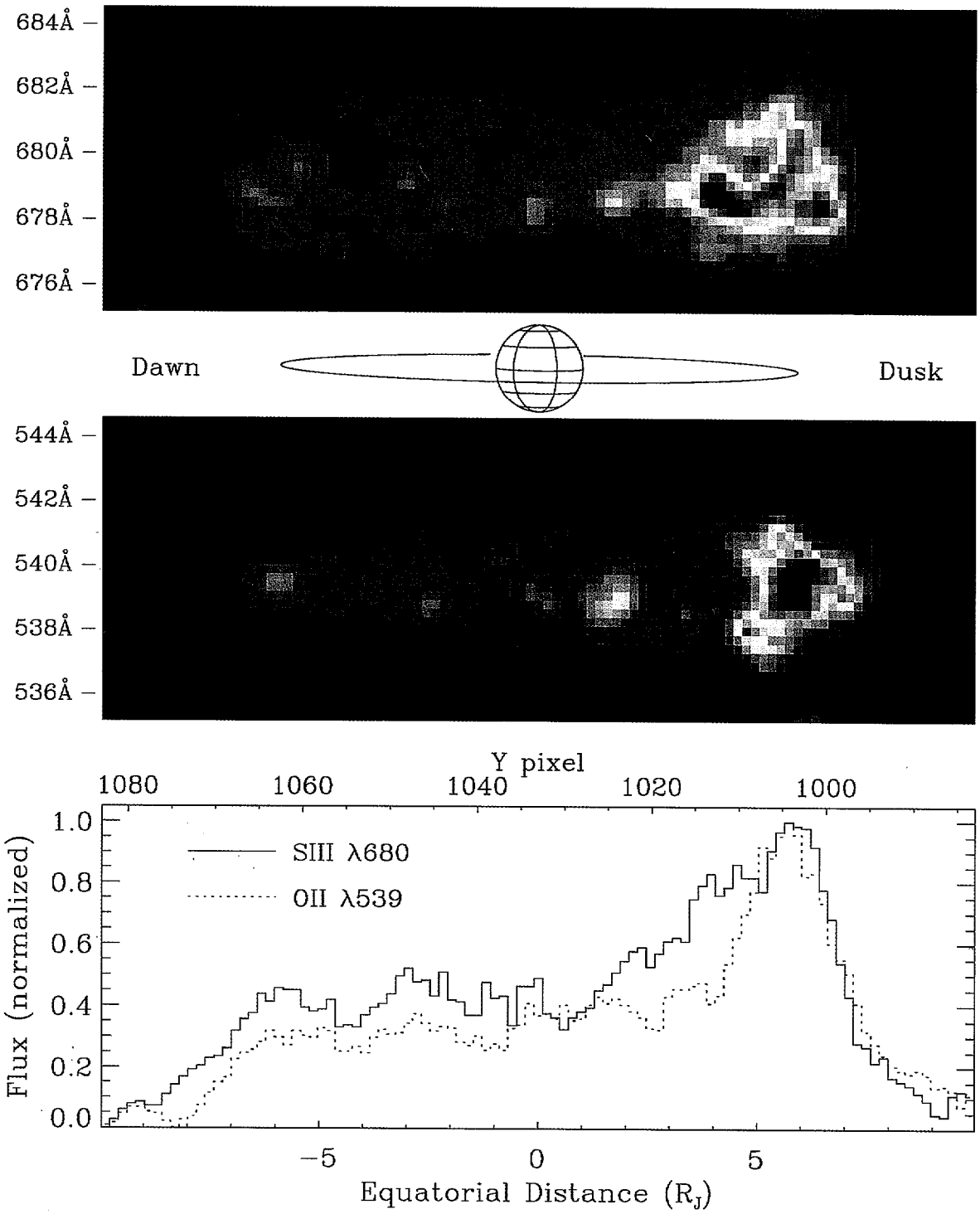

FIG. 2.—The distribution of flux for two *EUVE* spectral features. The top panel shows a false color image of S III λ680, with a cartoon of Jupiter and Io's orbit drawn to scale below. The lower image is O II λ539. Regions with no emission are shown as dark blue, and bright emission regions are shown as dark red. The spatial imaging direction of the *EUVE* long wavelength detector (i.e., the *y*-pixel direction) is parallel to Jupiter's equatorial plane. The spectral dispersion direction (along *x*-pixels) is perpendicular to this, and wavelengths are shown on the left of each image. The bottom panel shows the flux summed along *x*-pixels. Both emissions are distinctly brighter on the dusk side of the planet. The images are smoothed over 3 × 3 pixel regions; the flux distributions shown at the bottom are smoothed over 5 *y*-pixels.

HALL et al. (see 426, L51)